Continuum Mech. Thermodyn. (2016) 28:1905–1924
DOI 10.1007/s00161-016-0518-x

ORIGINAL ARTICLE

Ruiping Zhang · Xiaoqing Zhang · Giulio Lorenzini · Gongnan Xie

Material combinations and parametric study of thermal and mechanical performance of pyramidal core sandwich panels used for hypersonic aircrafts

Received: 22 March 2016 / Accepted: 24 June 2016 / Published online: 12 July 2016

Abstract A novel kind of lightweight integrated thermal protection system, named pyramidal core sandwich panel, is proposed to be a good safeguard for hypersonic aircrafts in the current study. Such system is considered as not only an insulation structure but also a load-bearing structure. In the context of design for hypersonic aircrafts, an efficient optimization should be paid enough attention. This paper concerns with the homogenization of the proposed pyramidal sandwich core panel using two-dimensional model in subsequent research for material selection. According to the required insulation performance and thermal–mechanical properties, several suitable material combinations are chosen as candidates for the pyramidal core sandwich panel by adopting finite element analysis and approximate response surface. To obtain lightweight structure with an excellent capability of heat insulation and load-bearing, an investigation on some specific design variables, which are significant for thermal–mechanical properties of the structure, is performed. Finally, a good balance between the insulation performance, the capability of load-bearing and the lightweight has attained.

Keywords Pyramidal core sandwich · Thermal · Mechanical · Material combinations · Load-bearing

Abbreviations

b	Thickness of the lattice-frame (mm)
B_t	Thickness of the top face sheet (mm)
C	Specific heat [J/(kg K)]
E	Young's modulus (Pa)
F	Force (N)
G	Modulus of rigidity (Pa)
H	Thickness of thermal insulation sample (mm)

Communicated by Andreas Öchsner.

R. Zhang · G. Xie (✉)
Department of Mechanical and Power Engineering, Northwestern Polytechnical University, P.O. Box 24, Xi'an, Shaanxi 710072, China
E-mail: xgn@nwpu.edu.cn

X. Zhang
Air-Breathing Hypersonic Technology Research Centre, China Aerodynamics Research and Development Centre, Mianyang 621000, Sichuan, China
E-mail: mukai_zhang@126.com

G. Lorenzini
Department of Industrial Engineering, University of Parma, Parco area delle Scienze 181/A, 43124 Parma, Italy
E-mail: giulio.lorenzini@unipr.it

k	Thermal conductivity [W/(m K)]
l	Half the length of the cross in the pyramidal core structure (mm)
T	Temperature (K)
T_t	Thickness of the top face sheet (mm)
t	Thickness of the cross in the pyramidal core structure (mm)
t'	Thickness of the upper part of the cross (mm)
q_r	Local radiation heat flux (W/mm^2)

Greek symbol

β	A non-dimensional thermal diffusivity
σ	Stress (Pa)
ε_{ij}	displacement (mm)
γ	Ratio between the rate of the heat conduction and the rate of the thermal energy storage of the homogenized core (–)
ε	Surface emissivity (–)
μ	Poisson's ratio (–)
τ	Shear stress (Pa)
θ	The inclined angle of lattice-frame (°)
ρ	Density (kg/m^3)

Subscripts

i, j	i, j Represent the direction for x, y, z
r	Radiation
t	Thickness (mm)

1 Introduction

Hypersonic aircrafts are capable of flying at the speed from Mach number of 5 to Mach number of 10; however, they suffer from a potentially serious safety problem under harsh and complex situations. To achieve a successful hypersonic flight, aircrafts should be designed to withstand extremely high aerodynamic heating and aerodynamic loads encountered on outer walls of aircrafts. In addition, non-uniform temperature distribution induced by the "aerodynamic heating" on different parts of aircrafts should cause a thermal gradient and thus induces a large thermal stress, resulting in a huge damage for hypersonic aircrafts. Therefore, thermal protection systems (TPSs) are proposed to protect the fuselage of hypersonic aircrafts from serious thermal, aerodynamic and impact loads. Particularly, the leading edges and nose cone of hypersonic aircrafts require the most sophisticated TPSs, since they experience much larger thermal and structural loads [1].

There are three kinds of TPSs: passive TPSs, semi-active TPSs and active TPSs. Among them, passive TPSs are adopted because of the safest, most practical and lightest characteristics. An amount of related researches have been done in the past years. For examples, Spinnler et al. [2] modeled the combined conduction and radiation heat transfer through porous materials to predict the temperature distribution and heat transfer in insulations comprised of the materials separated by multiple screens. The experimental results were compared with theoretical predictions to evaluate the effectiveness of the screens to reduce the effective thermal conductivity of the insulations. Fatemi and Lemmen [3] applied equivalent thermal and mechanical properties of a honeycomb core into a laminate shell structure and showed the reasonably accurate thermo-mechanical behavior and considerably decreased the computational costs of the finite element analysis. The minimal boundary conditions concept was applied by Hütter et al. [4]. The unconstrained micromorphic constitutive law of an elastic porous medium was obtained by the homogenization. It was shown that the model was consistent with the Germain's homogenization concept for microscale media. Gori et al. [5] evaluated the effective thermal conductivity of an ablative composite material in the state of virgin material and in three paths of degradation. Ferraiuolo and Manca [6] built novel analytical/numerical methodologies to evaluate the temperature distribution in a multilayered structure. The integral method was precisely developed solving the non-homogeneous nonlinear partial differential equation for multilayered bodies. Xie et al. [7] introduced an idea combining a transient heat transfer model and an efficient optimization model for multilayer insulation of TPS. It was found

that the usage of multilayer insulation materials for the TPS could save more than 17 % weight compared with a single-layer TPS. Ji et al. [8] investigated the impact of the layout, the number and the locations of the foils, as well as the density of the insulation on the insulation performance of multilayer thermal protection. Li et al. [9] developed a nonlinear pyrolysis layer model and then presented two kinds of novel designs of charring composites, simulated and compared their thermal behaviors. Kumar and Mahulikar [10] presented an explicit finite-difference scheme for analysis of one-dimensional transient heat transfer in a multilayer TPS. Advanced lightweight ablative materials developed at the NASA Ames Research Center were used to design a lightweight thermal protection system. Huo et al. [11] investigated aerothermoelastic response of a C/SiC panel which was a primary structure for ceramic matrix composite single thermal protection system for hypersonic vehicles. Vaz et al. [12] addressed a finite strain thermo-elastic-plastic formulation which fully coupled to the energy conservation equation and investigated the sensitivity of the mechanical response with respect to the temperature evolution based on tensile tests for small to moderate temperatures.

In recent years, the feasibility of increasing the heat transfer rate by filling, completely or partially, the heat transfer device with a porous medium has been considered [13]. Therefore, the considerable efforts have been focused on developing integral thermal protection system (ITPS). ITPS insulates the vehicle from aerodynamic heating as well as carries primary vehicle loads. It is multifunctional and lightweight to adopt such a structure. An ITPS configuration offers not only insulation but also load-bearing capabilities and requires low maintenance. The panels can be large in size, thus reducing the number of panels needed [17]. The stretch-dominated LFM structure is about 10 times stiffer and 3 times stronger than the bending governed metal foams at the same porosity level [14].

Evolutionary structural optimization (ESO) method was performed by Prithivirajan et al. [15] with the removal of inefficient elements from the design domain to evolve the structure toward the optimum. Martinez et al. [16] developed a micromechanical method to homogenize the sandwich panel and calculated the equivalent thermal forces and stresses in an ITPS subjected to mechanical and thermal loads. For a novel cellular configuration—hexagonal–rectangular honeycomb in multifunctional applications, Bezazi et al. [17] described the properties of mechanical in-plane and thermal conductivity. An integrated thermal protection system for spacecraft reentry on a corrugated core sandwich panel concept fulfilling both thermal and structural functions was optimized for minimal mass by Gogu et al. [18]. Martinez et al. [19] developed a micromechanical method to homogenize the sandwich panel as an equivalent orthotropic plate and calculate the equivalent thermal forces and moments for a given temperature distribution. Ravishankar et al. [20] performed the homogenization of a new concept for an ITPS panel as a two-dimensional (2D) orthotropic plate. A representative volume element/unit-cell of the panel was analyzed to obtain the equivalent stiffness properties of the 2D plate. Jänicke et al. [21] paid special attention to the description of size-dependent microtopological effects. They focused on the relevance of extended continuum theories describing the local deformation state of microstructural materials and therefore introduced a homogenization scheme for two-scale problems replacing a heterogeneous Cauchy continuum on the microscale by a homogeneous effective micromorphic continuum on the microscale. Liu et al. [22] determined the effective mechanical properties of the honeycomb core adopting mechanics of materials method, and the effective properties were then used with classical laminate theory to construct an equivalent laminate plate to simulate the response of three-dimensional honeycomb core structure. Xie et al. [23] had chosen the corrugated sandwich panel as the optimization problem to design an integrated thermal protection system for minimum weight. The objective function was the mass per unit area of the ITPS, and the temperature and total stress both must be below specific values were set as the constraint. Arabnejad et al. [24] adopted asymptotic homogenization as a benchmark to test the accuracy of alternative schemes of homogenization applied to lattice materials. AH was first applied to determine the effective elastic moduli and yield strength of six lattice topologies for the whole range of relative density. Jiang et al. [25] proposed five different layouts for the insulation layer of the ITPS: bounded/unbounded foam with blade stiffeners or hat-section stiffeners, as well as simple bounded foam. Figures of Merits (FoMs) weighing the combination of load-bearing capability and the mass of ITPS were built. The optimization objective functions were created to consider the insulation performance, structural strength and stiffness. Based on simulated annealing algorithm, Zhao et al. [26] proposed a multidisciplinary optimization procedure to unveil the minimum weight design for one-layer and two-layer corrugated core sandwich panel subjected to in-service thermal and mechanical loads. Cheng et al. [27] established a theoretical predictive model to achieve the equivalent thermal conductivity of a lattice core sandwich structure by considering both the heat conduction and radiation.

To perfect the insulation performance, a novel kind of lightweight integrated thermal protection system—pyramidal core sandwich panel is proposed in the current study. Compared with the adaptable, robust, metallic, operable and reusable TPS, the pyramidal core sandwich panel provides a higher capability in structural load-

bearing. After heat transfer analysis for the pyramidal core sandwich panel is performed, the thermo-mechanical performance of the structure is evaluated under thermal loads and specific aerodynamic loads. The significant considerations, such as specific strength (strength-to-weight ratio), tensile mechanical properties, fracture toughness, fatigue strength, low-speed impact strength, in material selection for the design of hypersonic aircrafts should be taken into account [28]. In the current research, several appropriate material combinations are selected for the pyramidal core sandwich panel according to the insulation performance and certain important thermal–mechanical properties which the thermal protection system should be satisfied. Then, for a lightweight structure with an excellent capability of heat insulation and load-bearing, some specific design variables which have significance for properties of the pyramidal core sandwich panel are investigated. In the meantime, a good balance between insulation performance, capability of load-bearing and lightweight can be attained.

2 Physical model and assumptions

Figure 1 schematically shows a pyramidal core sandwich panel characterized as ITPS (integrated thermal protection system). Pyramidal core sandwich panel consists of four parts: the top face sheet (TFS), lattice-frame (Pyramidal core), insulation material (Saffil fiber insulation) and the bottom face sheet (BFS). At the same exactly identical location, the heating rate during the entry period is obviously higher compared to the ascent period. In the ascent, the heating rate on the leeward and on the windward is very similar due to the constantly low attack angle. The peak heating value, as a function of distance from the vehicle nose, for the windward surface of the vehicle during the entry is represented in Fig. 2a. The peak heating value for the leeward during the entry is provided in Fig. 2b. Also, the peak heating value during the ascent is shown in

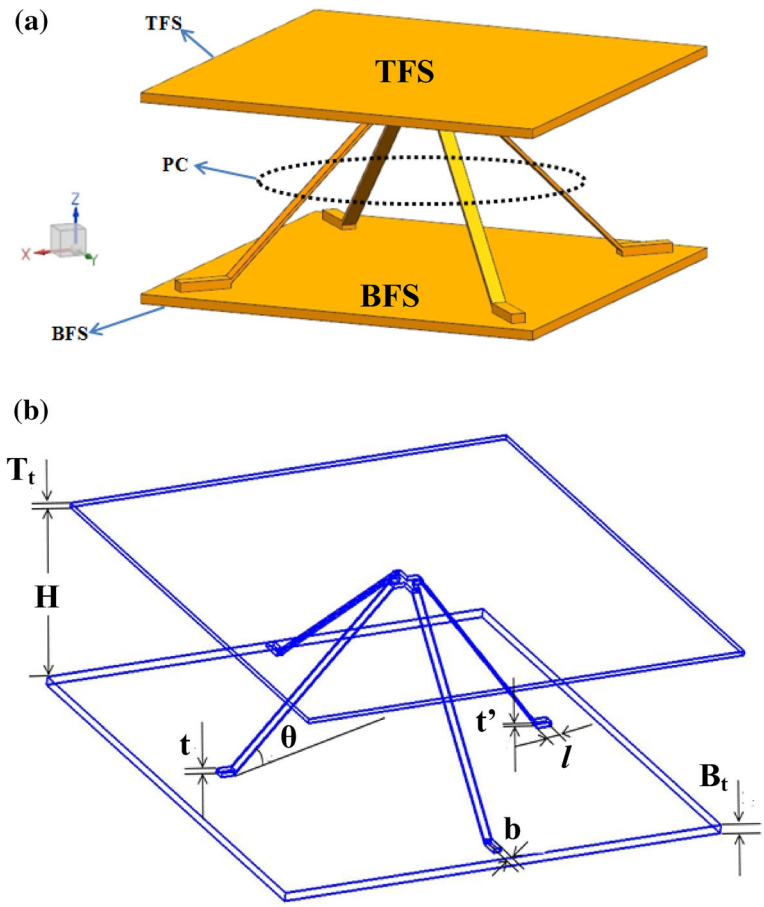

Fig. 1 Schematic diagram of geometrical model: **a** the typical pyramidal core sandwich panel for thermal protection thermal system consisting of top face sheet, pyramidal core and bottom face sheet; **b** the simplified geometry of the pyramidal unit-cell, two thin face sheets with the thickness of T_d and b_d, respectively, and pyramidal core with the inclined angel of θ

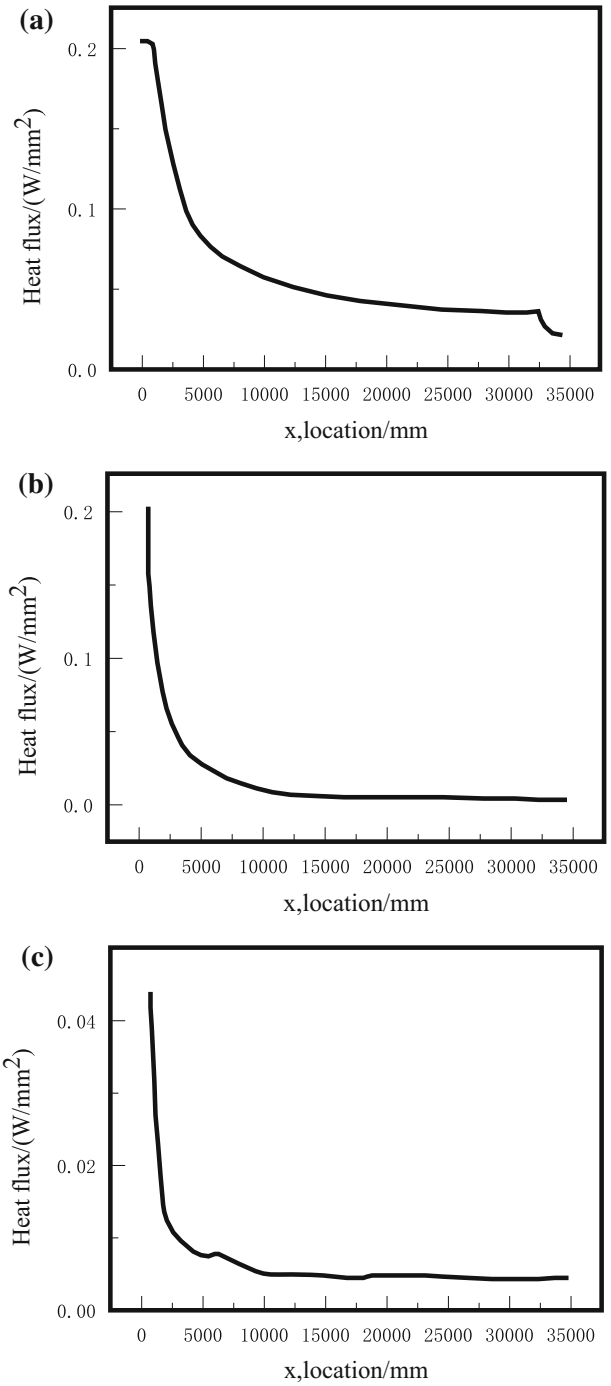

Fig. 2 Peak heating value as a function of distance from the vehicle nose for windward and leeward surface during the entry and ascent period: **a** the peak heating value for the windward during the entry; **b** the peak heating value for the leeward during the entry; **c** the peak heating value during the entry [28]

Fig. 2c. In the current paper, a location from the vehicle nose with distance of 264 in. is determined to select a typical heat flux used in analysis, as shown in Fig. 3.

The typical transient heat flux is applied on the top surface of the TFS as the initial temperature of the whole structure is assumed to be 295 K. As shown in Fig. 4, a considerable portion of heat is radiated out to ambient environment due to tremendous temperature difference between the ambient and the thermal protection structure, and then remaining heat is conducted to bottom face sheet through top face sheet, Saffil fibers as

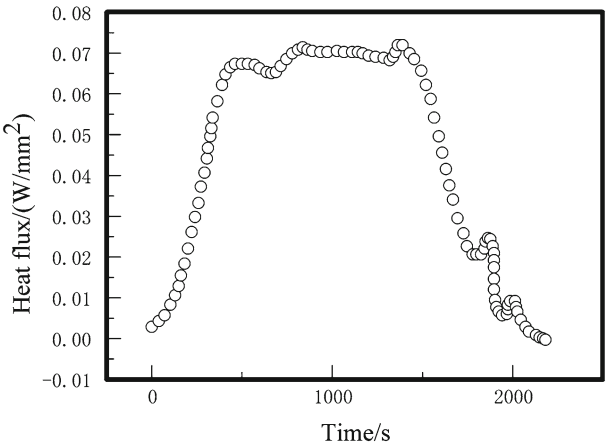

Fig. 3 Transient heat flux derived from the location of the vehicle nose with a value of 264 in. applied on hot boundary (*top surface*), the thermal load is referred to document [29]

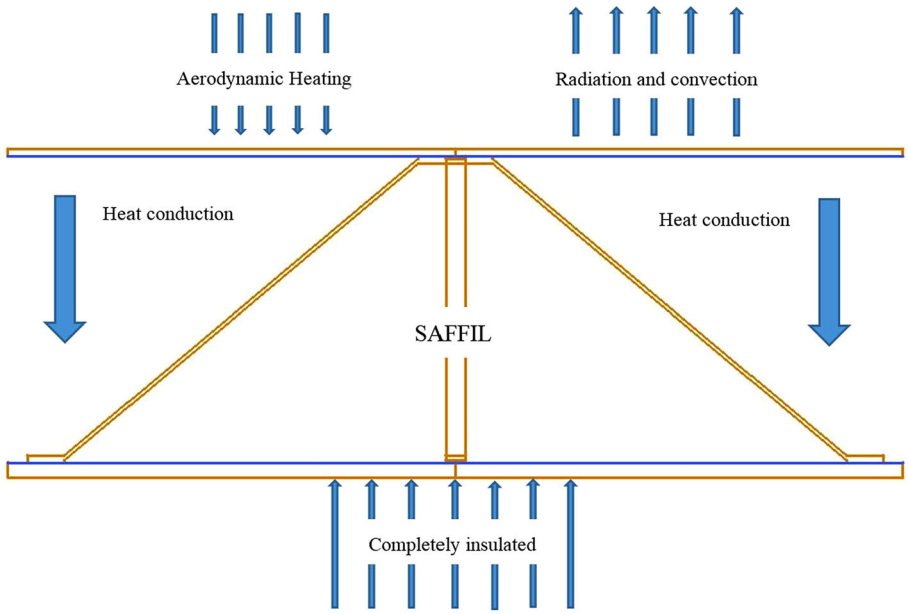

Fig. 4 Principles of the combined radiation and heat conduction transfer in the pyramidal core sandwich panel where the BFS is completely insulated, and the convection, radiation through Saffil can be ignored in the current paper

well as pyramidal core. The temperature at bottom of the structure should achieve a higher value if bottom surface cannot dissipate the heat energy. Therefore, a conservative assumption that the bottom face of the BFS is completely insulated is made for a more safe evaluation. This is the reason that there is still radiation and convection between the insulation materials due to its porosity. In our preliminary design, a convection and radiation through insulation material can be ignored. The insulation material is assumed to obstruct all the heat from the top face sheet to any part of the unit-cell. Another notable assumption is also proposed that there is no thermal contact resistance at interface between the face sheets, the lattice-frame and the Saffil fiber insulation.

The stress induced by aerodynamic load cannot be ignored when the influence of the parameters about the pyramidal core sandwich panels on insulation performance and load-carrying capability are investigated. Thus, the aerodynamic pressure should be taken into account. The aerodynamic pressure, which is comprised of the acoustic pressure and the local static aerodynamic pressure differential, is always assumed to be acting inward, whereas the acoustic pressure is oscillating to be acted inward or outward . The local static aerodynamic pressure differential consists of the local static pressure and the atmospheric pressure, as provided in Eq. (1).

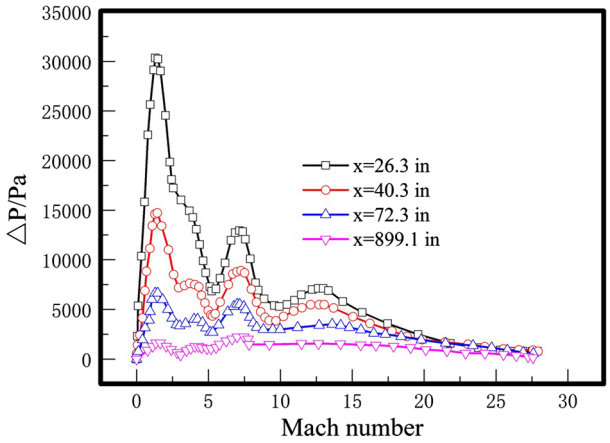

Fig. 5 Aerodynamic loads as a function of distance of the vehicle nose on the aircraft for the windward/leeward surface during the entry period

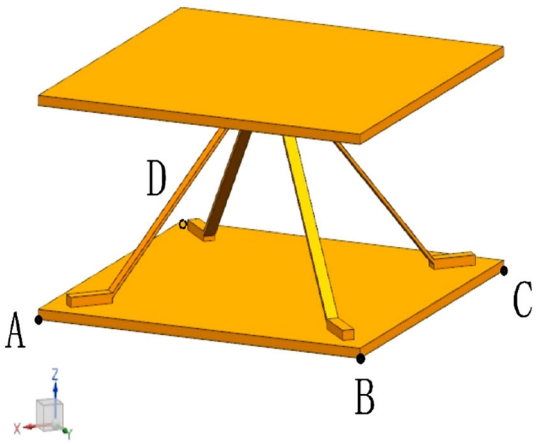

Fig. 6 Four feature points with specific constrains for displacement located in the bottom surface

The following two total pressures applied on the outer surface of the TPS are shown in Eqs. (2)–(3).

$$\Delta p_{\text{aerodynamic}} = p_{\text{local,static}} - p_{\text{atomspheric}} \tag{1}$$

$$\Delta p_{\text{ultimate,TPS}^+} = 1.4(\Delta p_{\text{aerodynamic}} + 3\Delta p_{\text{rms,acoustic}}) \tag{2}$$

$$\Delta p_{\text{ultimate,TPS}^+} = 1.4(\Delta p_{\text{aerodynamic}} - 3\Delta p_{\text{rms,acoustic}}) \tag{3}$$

where 1.4 is safety factor, and $\Delta p_{\text{rms,acoustic}}$ is the equivalent root-mean-square value of the pressure caused by acoustics which consists of engine acoustics and aerodynamic pressure in conditions of liftoff and ascent/entry relatively. The pressure induced by acoustics can be ignored in the present primary design process. As shown in Fig. 5, in the ascent and entry period, the aerodynamic pressure in the location from the vehicle nose with a value of 264 in. cannot exceed the value of 15,000 Pa.

To reduce the thermal mismatch problem which may result in large thermal stress, the bolts which impose specific displacement constraint on the connection between the cold structure and the hot structure are permitted to motion in a relatively free range. The constraints for displacement on four feature points are stated in Fig. 6 as follows: (1) The rotation for four points is permitted; (2) for point A, all degree of freedom except for the rotation around z axis is limited; (3) except for the movement along y axis and the rotation around z axis, other degree of freedom of point B is constrained; (4) point C is permitted to motion along x and y axis apart from the rotation around z axis; (5) except for the movement along x axis and the rotation around z axis, other degree of freedom of point D is constrained [28]. In the thermo-mechanical analysis, nothing but solid portion of the structure panel is taken into consideration, which includes the TFS, the BFS as well as lattice-frame. Taking Saffil insulation into account as a soft fibrous insulation with hardly any mechanical properties compared to the

solid portion mentioned above, the insulation material can be removed from all mechanical analysis without inducing any serious error.

3 Mathematical descriptions

3.1 Heat transfer equation

The numerical analysis problem turns out to be a nonlinear transient problem, which described as the following mathematical equation through a differential equation of heat conduction.

$$\frac{\partial}{\partial X}\left(k\frac{\partial T}{\partial X}\right)+\frac{\partial}{\partial Y}\left(k\frac{\partial T}{\partial Y}\right)+\frac{\partial}{\partial Z}\left(k\frac{\partial T}{\partial Z}\right)=\rho c\frac{\partial T}{\partial t} \tag{4}$$

where ρ, k, c represent density, thermal conductivity and specific heat of the insulation material, respectively, while t stands for time and T is temperature, X, Y, Z represent each directions of heat transfer.

Making a discretization for Eq. (1), the finite element equation of heat transfer is re-organized as follows:

$$[C(T)][T']+[K_{\mathrm{c}}(T)][T]=[Q(T)] \tag{5}$$

where K_{c} stands for the matrix of heat conduction, C stands for the matrix of specific heat, Q is the vector for heat flux of node, T and T' are the temperature vector of nodal and the derivative of the nodal temperature versus time, respectively. Each nodal transient temperature can be worked out by using the Newton–Raphson method to solve Eq. (2).

Equation (2) is subjected to the initial and boundary conditions as follows:

$$T(x,0)=T_0=295K \tag{6}$$

$$T(0,t)=T_1(t) \tag{7}$$

$$T(L,t)=T_2(t). \tag{8}$$

where T_0 represents the initial temperature of the whole lattice-frame sandwich structure, T_1 is the temperature load that applied on the top surface of the structure, T_2 is the temperature of the bottom surface, which contacts the underlying structure and needs to be within an acceptable temperature limit, and L is the thickness of the whole lattice-frame structure.

A large portion of heat is radiated out to the ambient by the upper surface of the top face sheet. The net thermal radiation is determined by the following equation:

$$q_{\mathrm{r}}=\varepsilon_{\mathrm{s}}\sigma_{\mathrm{s}}\left(T_t^4-T_{\mathrm{a}}^4\right) \tag{9}$$

where q_{r} stands for radiant heat flux, ε_{s} is the emissivity of the top surface, σ_{s} is the Stefan–Boltzmann constant of $5.67\mathrm{E}^{-8}\mathrm{W}/(\mathrm{m}^2.\mathrm{K}^4)$, T_t is the temperature of the top face sheet, and T_{a} is the ambient temperature.

3.2 Thermo-mechanical analysis model

On the bases of linear thermal stress theory, the equation about the relationship between thermal strain and thermal stress is correlated as follows:

$$\begin{cases}\varepsilon_x=\frac{\partial u}{\partial x}=\frac{1}{E}[\sigma_x-\mu(\sigma_y+\sigma_z)]+\alpha\Delta T\\ \varepsilon_y=\frac{\partial v}{\partial y}=\frac{1}{E}[\sigma_y-\mu(\sigma_z+\sigma_x)]+\alpha\Delta T\\ \varepsilon_z=\frac{\partial w}{\partial z}=\frac{1}{E}[\sigma_z-\mu(\sigma_x+\sigma_y)]+\alpha\Delta T\end{cases} \tag{10}$$

$$\gamma_{xy}=\frac{\tau_{xy}}{G},\gamma_{yz}=\frac{\tau_{yz}}{G},\gamma_{zx}=\frac{\tau_{xx}}{G} \tag{11}$$

where ε_x, ε_y, ε_z are the normal strains, γ_{xy}, γ_{yz}, γ_{xz} are the shear strains, u, v, w stands for displacements toward the direction for x,y, z axis, respectively. σ_x, σ_y, σ_z are the corresponding normal stress, τ_{xy}, τ_{yz}, τ_{xz}

are the shear stresses corresponding to γ_{xy}, γ_{yz}, γ_{xz} respectively, α is the thermal expansion, while ΔT is difference of temperature. E is Young' s modulus, and μ represents Poisson's ratio.

According to the generalized Hook's law, the above equation can be re-organized by thermal strain expression as:

$$\begin{cases} \sigma_x = 2G\varepsilon_x + \lambda e - \beta\Delta T \\ \sigma_y = 2G\varepsilon_y + \lambda e - \beta\Delta T \\ \sigma_z = 2G\varepsilon_z + \lambda e - \beta\Delta T \end{cases} \tag{12}$$

$$\tau_{xy} = G\gamma_{xy}, \tau_{yz} = G\gamma_{yz}, \tau_{xz} = G\gamma_{xz} \tag{13}$$

where

$$e = \varepsilon_x + \varepsilon_y + \varepsilon_z, \quad \lambda = \frac{\mu E}{(1+\mu)(1-2\mu)}, \quad G = \frac{E}{2(1+\mu)}, \quad \beta = \frac{\alpha E}{1-2\mu} \tag{14}$$

The equilibrium differential equation of thermo-elasticity, which is based on the equilibrium equation for elastic mechanics, is derived according to the thermal stress and thermal strain expression mentioned above as follows.

$$\begin{cases} (\lambda + G)\frac{\partial e}{\partial x} + G\nabla^2\mu - \beta\frac{\partial(\Delta T)}{\partial x} + F_x = 0 \\ (\lambda + G)\frac{\partial e}{\partial y} + G\nabla^2\mu - \beta\frac{\partial(\Delta T)}{\partial y} + F_y = 0 \\ (\lambda + G)\frac{\partial e}{\partial z} + G\nabla^2\mu - \beta\frac{\partial(\Delta T)}{\partial z} + F_z = 0 \end{cases} \tag{15}$$

F_x, F_y, F_z stands for volume force per volume along x, y, z axis, respectively, while ∇^2 is Laplace operator.

All basic equations and boundary conditions in the study of linear thermal elasticity are linear. Therefore, such problem could be solved separately when the temperature load and the aerodynamic load are applied on the sandwich structure, then the two results are added up. In the first step, the temperature distribution of the structure can be obtained by applying typical transient flux. Then the temperature value at some practical time point is chosen to be as a kind of "uncritical load," which is compared to the pressure load correspondingly, to calculate the displacement at the time point. Finally, the according strain and stress could be obtained through the above relationships.

4 Initial design and model validation

The size of pyramidal core sandwich panel is determined and given in Table 1. Also, materials of the outer panel and lattice-frame both are determined with aluminosilicate/Nextel 720 fiber composite, Epoxy/carbon fiber laminate is selected as the material of the inner panel, while the Saffil fiber insulation is chosen for the insulation material. The BFS's maximum temperature cannot exceed a value of 450 K that required for the underlying structure. The comparison about temperature in hot boundary between results in theory and simulation results from Ref. [30], as provided in Fig. 7a. It can be seen clearly that insulation performance of the FE model can satisfy these requirements. The radiation equilibrium temperature which mainly depends on the incident flux applied on the aircraft and the emissivity of the top surface of the panel represents the results in theory. The deviation between them is relatively obvious, but the future of trend is extremely identical. Considering the simplification of FE model for reducing the computational costs and some assumptions for a conservative result, such as the bottom surface is assumed to be perfectly insulated. Figure 7b shows a comparison in temperature variation of cold boundary between the simulation and the reference. Although the deviation is slightly obvious, the feature and trend of curves can be almost identical. Thus, the deviation is expected and acceptable and the given model can be safely applied in further research in the following sections.

5 Selection for material

5.1 Three-dimensional and two-dimensional FE models

To reduce the computational time for the transient heat transfer analysis considerably, the three-dimensional model can be simplified to a two-dimensional model. A comparative study between 2D model and 3D model was performed to prove the accuracy of using 2D model rather than 3D model. The 2D heat transfer model is shown in Fig. 8.The core of the pyramidal core sandwich panel is homogenized, while the top and the bottom

Table 1 Selected materials according to the capability of heat insulation and load-bearing [31]

Material	Epoxy/carbon fiber quasi-isotropic laminate	Nickel-chromium alloy, inconel 718	Alum- inosilicate/Nextel 720 fiber composite, quasi-isotropic woven	
Mechanical properties				
Density (kg/m^3)	1550–1580	8150–8300	2450–2600	
Young's modulus (GPa)	49.7–60.1	195–205	133.5–139.1	
Compressive strength (MPa)	542.1–656.8	1010–1240	67.9–68.8	
Tensile strength (MPa)	248.6–355.9	1220–1510	67.9–68.8	
Fracture toughness (MPa m$^{0.5}$)	6.12–87.61	120–150	40.5–47.6	
Poisson's ratio	0.305–0.307	0.28–0.3	0.23–0.25	
Thermal properties				
Max. service temperature (K)	413–493	1130–1255	1273–1373	
Melting point (K)	373–453	1533–1610	1273–1373	
Specific heat (J/kg K)	901.7–1037	410–455	950–1100	
Thermal conductivity (W/m K)	1.28–2.6	10.5–12.5	2.52–2.93	
Thermal expansion (μstrain/K)	0.36–4.02	11.5–13.5	5.745	
Material	Zirconia	Titanium	Beryllium	Cast aluminum alloy
Mechanical properties				
Density (kg/m^3)	6080–6210	4407–4451	1850	2755
Young's modulus (GPa)	210–220	110–117	305	68–88.5
Compressive strength (MPa)	1429–1575	758–1170	250–365	30–280
Tensile strength (MPa)	1429–1575	896–1138	320–430	75–360
Fracture toughness (MPa m$^{0.5}$)	15–20	82–100	10–14	18–35
Poisson's ratio	0.24–0.31	0.32	0.06–0.075	0.34
Thermal properties				
Max. service temperature (K)	1248–1298	630–672	803–1103	403–473
Melting point (K)	2823–2973	1878–1933	1545–1565	723–980
Specific heat (J/kg K)	418–436	553–575.6	1820–1930	944–982
Thermal conductivity (W/m K)	1.8–1.9	7.3–7.9	190–216	80–220
Thermal expansion (μstrain/K)	7.8–8.1	9–9.46	10–12	16–24

face sheets remain the same as those of 3D model. The properties of the homogenized core are calculated by the rule of mixtures formulae. The following formulae show the density, specific heat and thermal conductivity of the homogenized core [18].

$$\rho_c = \frac{p_1 V_1 + p_2 V_2}{V_c} \tag{16}$$

$$C_c = \frac{C_1 p_1 V_1 + C_2 p_2 V_2}{V_c C_c} \tag{17}$$

$$K_c = \frac{k_1 A_1 + k_2 A_2}{A_c} \tag{18}$$

where ρ is density, C stands for specific heat and k for thermal conductivity. The subscripts 1 and 2 relatively stand for insulation material and lattice-frame, while C stands for the homogenized core. A1 stands for the cross sectional area of space insulation material occupied and A2 represents the cross area of heat conduction path. Obviously, AC is the cross sectional area of homogenized core. Three future points are selected to prove the accuracy of the 2D FE model. Figure 9 plots the temperature with time on the TFS, the middle of the structure and BFS by using 2D model and 3D model, respectively. It can be clearly seen that both results obtained by adopting two methods in three locations chosen for validation are extremely identical. Therefore, the presented 2D model is testified to be reliable in predicting temperature variation at all locations for the whole sandwich structure.

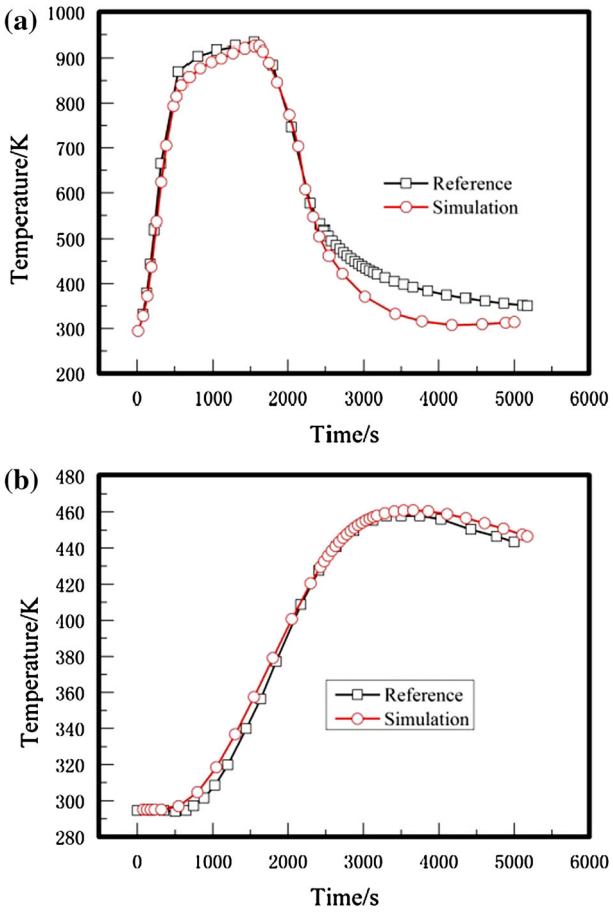

Fig. 7 Comparison of temperature with respect to time between reference results [30] and predicted results: **a** the temperature variation in the TFS; **b** the temperature in the BFS. (The trend and feature are almost the same between the predicted results and the simulation results)

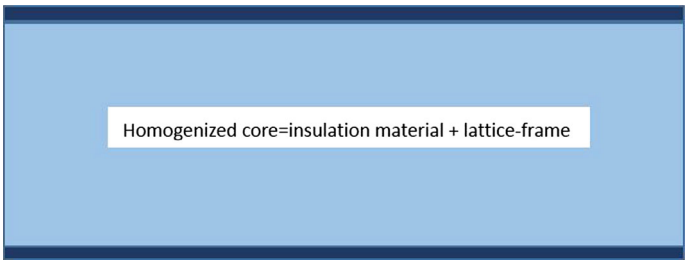

Fig. 8 Equivalent 2D heat transfer model of which the core of the pyramidal core sandwich panel is homogenized, while the top and the bottom face sheets remain the same as in the 3D model

5.2 The approximate response surface for temperature

Using the previous FE model we constructed to test different material combinations one after another is improper due to a considerable number of computational costs. Also, an approximate response surface should be fitted through considerable samples which will be used in the following optimal sections. To lower difficulty in obtaining approximate response surface, less parameters are required to express the approximate function of maximum temperature in the BFS. The thermal FE model discussed in the previous section involves 9 material parameters (specific heat C, thermal conductivity k and density ρ for the TFS, BFS and lattice-frame). The emissivity of the TFS which mainly depends on the coating of the surface rather than the material of TFS, and ε of 0.86 is determined in the current paper. We used non-dimensionalization to make a mildly simplified analytical model of the thermal problem together with a global sensitivity analysis. The properties of the TFS

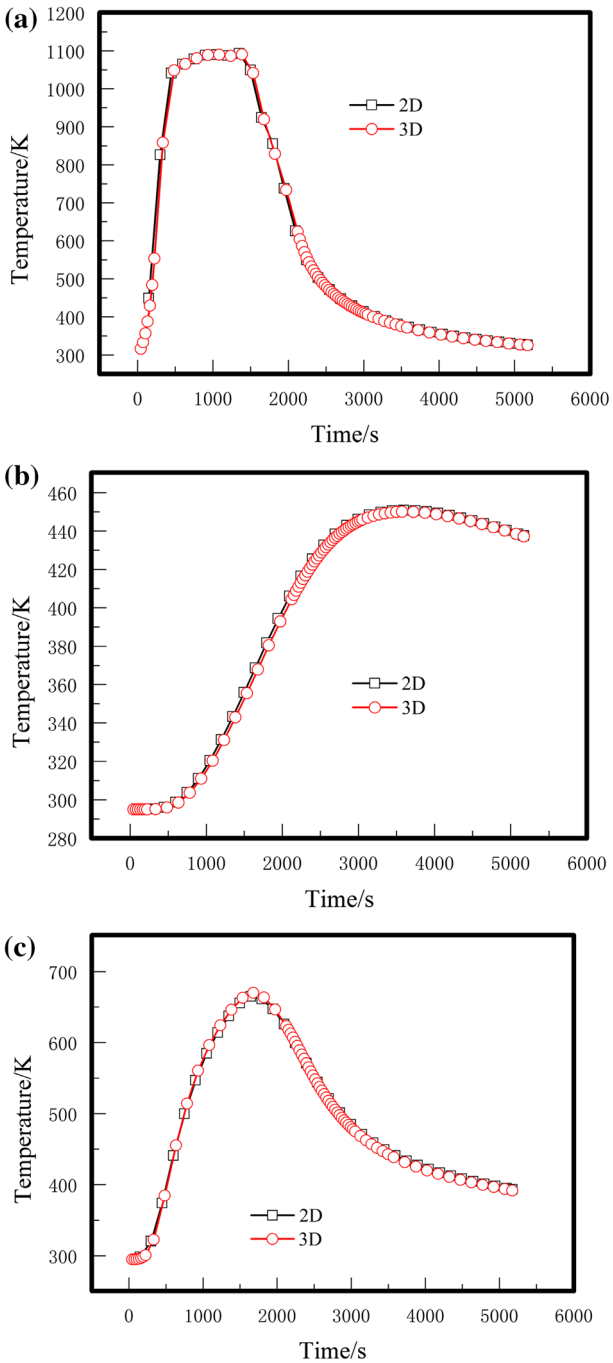

Fig. 9 Comparison of temperature with respect to time of 2D model and 3D models: *a* temperature on the TFS; *b* temperature on the middle of the structure along z axis; *c* temperature on the BFS

have a little impact on temperature distribution of the whole structure due to the small thickness of the out wall. We can find out that the maximum temperature in the BFS with an approximate response surface as a function of only two non-dimensional parameters, β and γ. The function is provided as follows [22]:

$$\beta = \frac{\frac{k_C t_{\text{end}}}{d_C}}{d_C \rho_C C_C} = \frac{k_C t_{\text{end}}}{d_C^2 \rho_C C_C} \tag{19}$$

$$\gamma = \frac{d_B \rho_B C_B}{d_C \rho_C C_C} \tag{20}$$

According to Eq. (4), parameter β, a non-dimensional thermal diffusivity, is proposed which can be considered as the Fourier number. β is the ratio between the rate of the heat conduction and the rate of the thermal energy storage of the homogenized core. With the increase of β, the temperature at all points in the structure tend to be further uniform in the process of non-steady heat conduction. Also, γ which is the ratio between the heat capacity of the BFS and the heat capacity of the homogenized core is proposed.

To reduce the calculation time, t_{end} in β and d_{B} in γ is altered to get some sample points to fit an approximate response surface for temperature. The considerable 170 finite simulations are carried out, and the temperature approximate function with a method of polynomial is calculated between these points. It is necessary to check out whether a function of only β and γ can also express the accurate maximum temperature in the BFS with a good accuracy obtained from finite models. Then, 120 Latin hyper-square points which fall in the range used for $\beta \in [0.17, 2.50]$ and $\gamma \in [1.017, 2.01]$ are chosen to validate the temperature function mentioned above. The mean of absolute value of deviation between the finite element analysis models and the predictions of the temperature is 6.61 K, while the maximum absolute difference for both is 32.95 K but the relative high value fall into the range of β and γ which can be ignored. A polynomial is fitted to select appropriate material combinations from the perspective of heat insulation, also, β and γ are used to analyze the maximum temperature variations with different geometric size in the BFS.

5.3 Material selection in preliminary

Lightweight is our main goal in designing thermal protection system except for capability of insulation and load-bearing. Therefore, the equivalent density of the whole structure is required to be lower. The maximum density cannot excess the value of 9000 kg/m^3. The maximum service temperature of the TFS is required to be above 1200 K due to the maximum radiation equilibrium temperature in the TFS reaching a general value of 1100 K typically. The lattice-frame has to resist very high temperature due to the connection with the TFS at the upper part. The maximum service temperature of the lattice-frame should be identical with the TFSs. The BFS should act as a heat sink, and its temperature is required to be below a value of 450 K (which is a typical limit temperature for aluminum material of the underlying structure). Every part of the pyramidal core sandwich structure should be responsible for load-bearing. Young's modulus should be no less than 50 GPa. The TFS, as the outer wall of the supersonic aircrafts, should have to withstand potential impact which has to be translated into a more serious control of selection for fraction toughness. The fracture toughness of the TFS should achieve the value of 20 MPa m$^{0.5}$. And the fracture toughness of the remaining parts of the pyramidal core sandwich structure must arrive at the fracture toughness value of 10 MPa m$^{0.5}$.

In conclusion, nickel-chromium alloy and aluminosilicate/Nextel 720 fiber composite have been chosen as the candidate material for the TFS. Epoxy/carbon fiber quasi-isotropic laminate, beryllium grade S-200F, titanium alloy and cast aluminum alloy have been selected for the material of the BFS, while zirconia has been chosen for the lattice-frame. The thermal and mechanical properties of these materials are provided in Table 1. Actually, the material for the TFS is suitable for any part of the structure. Large difference of CTE (coefficient of thermal expansion) between adjacent parts of the whole structure can induce relatively large thermal stress. The materials with similar properties in CTE should be combined into a group. On the condition that the size of the structure with different material combinations mentioned above is fixed, the maximum temperature at the BFS is all below 450 K which is safe for the underlying structure. Also, considering the properties of tensile/compressive strength which should be satisfied, four suitable material combinations are selected as candidates for following optimization process. In general, the material combination is provided in Table 2.

Table 2 Four material combinations for heat insulation and load-bearing

TFS	Lattice-frame	BFS	T_{max} (K)
Aluminosilicate/Nextel 720 composites	Aluminosilicate/Nextel 720 composites	Aluminosilicate/Nextel 720 composites	405.373
Inconel 718 alloy	Zirconia	Zirconia	404.789
Inconel 718 alloy	Zirconia	Titanium alloy	408.693
Inconel 718 alloy	Zirconia	Beryllium	384.684

Table 3 Initial design variables of the structure used in the material selection process

Design variable	B_t/m	T_t/m	H/m	b/m	l /m	t/em	t°/m	θ (°)
Size	0.006	0.003	0.125	0.008	0.015	0.003	0.002	40

Table 4 Maximum temperature in the BFS and stress induced by heat flux and aerodynamic load with the variation of θ

Angle of lattice-frame (°)	Temperature/K	Thermal stress/(MPa)	$\text{Stress}_{15,000\,\text{Pa}}$/(MPa)	$\text{Stress}_{30,000\,\text{Pa}}$/(MPa)	Relative density/(kg/m^3)
30	405.007	3.797	101.144	200.612	218.979
35	404.489	4.091	52.6073	104.778	219.954
40	405.373	3.429	45.5258	92.292	220.165
45	405.027	4.118	31.420	63.748	220.874
50	404.845	6.776	22.036	41.338	221.697
55	405.008	4.314	18.597	34.650	222.680
60	404.988	4.944	16.003	29.588	223.890

6 Results and discussion

6.1 Effect of θ on the thermal–mechanical properties of the structure

A typically initial size values are set as original value for the following study, as provided in Table 3, and then one of the parameters is altered in a reasonable range to investigate the influence of geometric parameters on the thermal–mechanical capability of the pyramidal core sandwich panel. The maximum temperature in the BFS cannot be considered as the only objective for our study for optimization of the structure, but also the weight of the whole structure and the stress induced by heat flux and aerodynamic load. In the primary research, aluminosilicate/Nextel 720 composites are chosen as the material of every part of the structure while Saffil is set as a candidate for the insulation material. The θ, angle of lattice-frame which belongs to the core of the structure, varied from 30 to 60°. According to the description for boundary conditions in Sect. 2, two conditions when only thermal load and additional aerodynamic load of 15,000 or 30,000 Pa are applied are considered. And with that, maximum temperature about heat insulation performance and strength for the whole structure are investigated, as shown in Table 4. The maximum thermal stress generated by only transient heat flux appears in the bottom part of the lattice-frame near the bottom panel with θ from 30 to 60°. Also, the stress produced by aerodynamic load mainly appears in for the lattice-frame; therefore, the thickness of the lattice-frame can be adjusted to attain more excellent thermo-mechanical capability for the pyramidal core sandwich panel, as shown in Fig. 10.

In consequence of Saffil's taking the responsibility of heat insulation mainly, the maximum temperature in the BFS almost maintains the same value of 405K in all circumstances of the variance of θ. The thermal stress hardly has any change, because the θ of lattice-frame has little impact on temperature distribution and geometric cross-sectional area is always identical. Also, it can be seen clearly from the Table 3 that the stress induced by both high thermal gradient and aerodynamic load decreases as the increment of θ. In the meantime, the relative density increases as the θ increase. To obtain a lightweight pyramidal core sandwich panel which possesses excellent mechanical properties, the weight and the stress induced by temperature gradient and aerodynamic load of 15,000 Pa are both considered as objectives for optimization of the structure. The correlations between two dependent variables and the independent variable are plotted in Fig. 11. When the angle of the lattice-frame is chosen in specific range from 40 to 45°, a good balance between weight and strength can be attained. The pyramidal core sandwich panel can be safely applied as thermal protection system above 35° of lattice-frame when aerodynamic load of 15,000 Pa is applied, and the structure is applicable for θ exceeding about 45° when 30,000 Pa is exerted.

6.2 Effect of B_t on the thermal–mechanical properties of the structure

To investigate the effect of B_t on the maximum temperature in BFS and the mechanical performance of the whole structure, the above-mentioned model is adopted again and the other geometric parameters is fixed at initial size mentioned above. The increment of the thickness of the TFS has little impact on the maximum temperature in the BFS due to the extremely thin thickness. Increasing the thickness of the BFS can improve

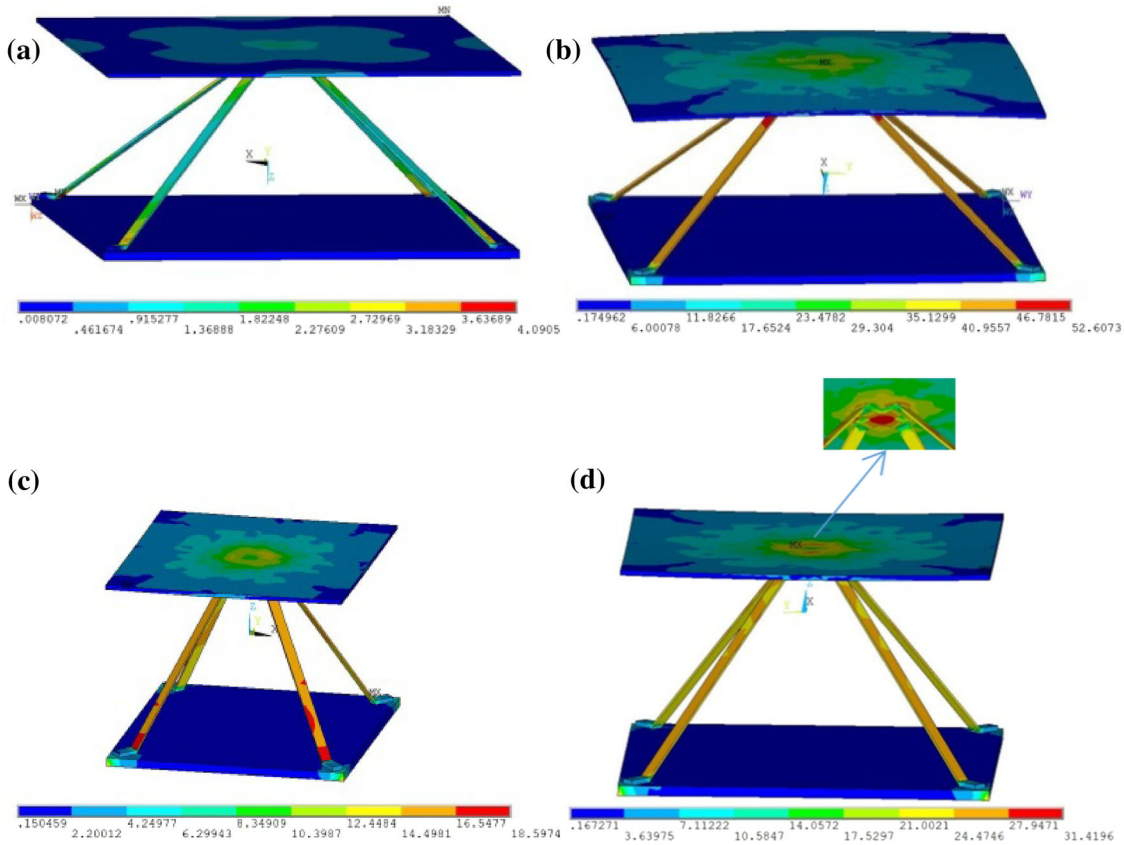

Fig. 10 Von Mises stress contour: **a** when only thermal load is applied to the pyramidal core structure (the maximum thermal stress appears in the bottom part of the lattice-frame near the BFS); **b** in the additional aerodynamic load of 15,000 Pa with the 35° of $\boldsymbol{\theta}$ (the maximum stress appears in the upper part of the lattice-frame); **c** in the additional aerodynamic load of 15,000 Pa with the 55° of $\boldsymbol{\theta}$ (the maximum stress appears in the lower part of the lattice-frame); **d** in the additional aerodynamic load of 15,000 Pa with the 45° of $\boldsymbol{\theta}$ (the maximum stress appears in the top part of the lattice-frame near the TFS)

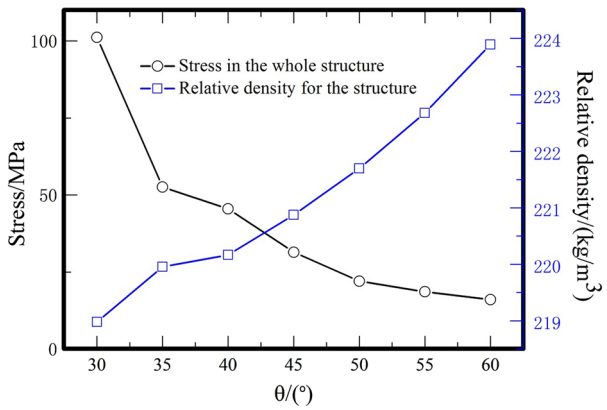

Fig. 11 By changing $\boldsymbol{\theta}$ in a reasonable range, the stress induced by aerodynamic load of 15,000 Pa and maximum temperature in the BFS generated by transient heat flux are investigated with consideration for lightweight

the insulation performance for the thermal protection system. More heat is absorbed by the bottom panel, and less heat energy reached the bottom surface of the bottom panel, as explained particularly in Eq. (11). According to Sect. 4, the lattice-frame is the relatively weak part of the whole thermal protection structure no matter that additional aerodynamic load is also applied on. In more detail, the maximum stress appears in the cross part of the lattice-frame or the lowest location of the lattice-frame, as studied in Sect. 4.

Table 5 Maximum temperature in the BFS and stress induced by heat flux and aerodynamic load with the variation of B_t

Thickness of BFS (mm)	Temperature/K	Thermal stress/(MPa)	$Stress_{15,000\,Pa}$ /(MPa)	$Stress_{30,000\,Pa}$ /(MPa)	Relative density/(kg/m^3)
4	437.387	5.760	38.321	72.267	185.963
5	420.459	5.065	32.173	66.091	203.550
6	405.027	4.118	31.420	63.748	220.873
7	393.268	3.327	31.534	63.936	237.945
8	384.471	3.344	31.484	63.837	254.758
9	376.710	2.974	31.489	63.830	271.329
10	369.968	2.804	32.610	66.566	287.660

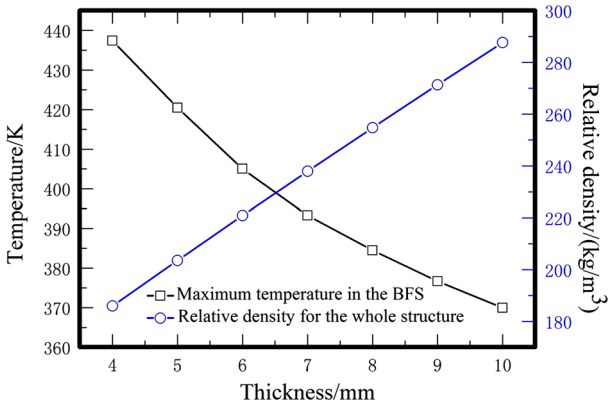

Fig. 12 By changing $\mathbf{B}_t$ in a reasonable range, the stress induced by aerodynamic load of 15,000 Pa and maximum temperature in the BFS generated by transient heat flux are investigated with consideration for lightweight

Table 6 Maximum temperature in the BFS and stress induced by heat flux and aerodynamic load with the variation of b

Thickness of lattice-frame (mm)	Temperature/K	Thermal stress/(MPa)	$Stress_{15,000\,Pa}$ /(MPa)	$Stress_{30,000\,Pa}$ /(MPa)	Relative density/(kg/m^3)
4	405.456	4.550	66.618	134.811	285.078
5	405.453	4.298	53.364	108.356	285.554
6	404.676	3.464	44.696	89.478	286.029
7	404.652	4.605	43.184	86.828	286.501
8	405.373	3.429	45.526	92.292	286.992
9	404.831	3.162	44.776	91.137	287.441
10	405.391	4.571	39.070	79.213	287.908

The increase of the thickness of the BFS can lower the maximum temperature in BFS, and the thermal stress is decreased similarly. Because the maximum stress appears in the connection between the lattice-frame and the BFS, the increment of B_t can reduce the thermal stress due to the reduction of thermal gradient. The thermal stress is relatively lower compared to the stress caused by both thermal and aerodynamic load. The stress barely changes for mainly appearing in the upper part of the core. When the thickness of the BFS is greater than 5mm, the thermal structure can be safely used to protect the aircraft from aerodynamic heating in aerodynamic load of 30,000 Pa. The thickness in range [4, 10] can be applicable in aerodynamic load of 15,000 Pa. The opposite relation with the increment of thickness between the temperature and the relative density of the structure can be clearly observed from Table 5. Also, an excellent balance between insulation performance and lightweight is achieved when 6.5 mm is chosen for the thickness of the BFS, as shown in Fig. 12.

6.3 Effect of b on the thermal–mechanical properties of the structure

When 40°C is chosen for the angle of the lattice-frame and 6.5 mm is for the thickness of the BFS, a better insulation performance and load bearing capability can be realized. Therefore, the thickness of the lattice-frame is varied from 4 to 10 mm to investigate the effect of b on the thermal–mechanical properties. The parameter b shows proportional to the ratio between the solid portion and the soft portion for the pyramidal core of the

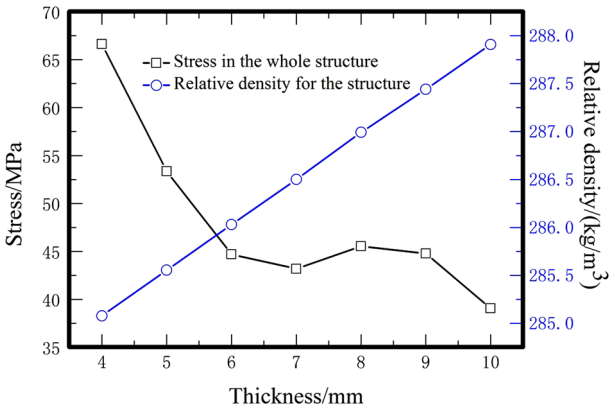

Fig. 13 By changing ***b*** in a reasonable range, the stress induced by aerodynamic load of 15,000 Pa and maximum temperature in the BFS generated by transient heat flux are investigated with consideration for lightweight

Table 7 Maximum temperature in the BFS and stress induced by heat flux and aerodynamic load with the variation of T_t

Thickness of TFS (mm)	Temperature/K	Thermal stress/(MPa)	$\text{Stress}_{15,000\,\text{Pa}}$ /(MPa)	$\text{Stress}_{30,000\,\text{Pa}}$ /(MPa)	Relative density/(kg/m^3)
2	403.347	3.832	91.661	185.122	202.836
3	405.373	3.429	45.526	92.291	220.165
4	406.349	2.963	34.455	68.609	237.238
5	408.473	2.511	34.448	67.469	254.060
6	409.396	2.290	34.291	67.431	270.636
7	410.734	2.067	34.107	67.339	286.972

structure, as shown in Table 6. As stated in Sect. 3.1, β and γ can determine the maximum temperature in the BFS. The variance of the thickness of the lattice-frame has little effect on the properties of the homogenized core; therefore, β and γ almost stay the same. In consequence, the maximum temperature in the BFS is hardly varied when different thickness of lattice-frame is settled.

The thermal stress generated by thermal gradient should be lower due to the increment of b. However, increase of volume of solid portion should cause a little increase of β which results in a further uniform temperature distribution, as explained in Sect. 3.1. When b is varied from 4 to 10 mm, the thermal stress is oscillating in a tiny range. In consequence, the size of lattice-frame should affect the stress induced by aerodynamic load due to lattice-frame's undertaking the responsibility of load-bearing, and the stress is decreased due to the increment of the cross-sectional area when the b falls in a range of [4, 7]. The stress has a slight oscillating trend in range of [7, 10] due to the oscillating trend of thermal stress. A good balance between load-bearing and lightweight can be attained when b of 6mm is selected for the thickness of the lattice-frame, as shown in Fig. 13.

6.4 Effect of T_t and l on the thermal–mechanical properties of the structure

Although the thickness of the TFS in a typical range has little impact on the maximum temperature in the BFS due to the thin thickness, the influence on the thermal and mechanical properties of the thermal protection structure caused by the thickness of TFS should be researched in detail. The capability of heat storage for the TFS will be improved with the increment of mass by increasing its thickness. Thermal resistance is considerably high for the part near the TFS which is relatively thin. Therefore, the temperature distribution turns to be more uniform with a relatively low speed. In consequence, the temperature in the top surface will be higher compared to the structure with large thickness for TFS. From time of about 2000s, the tendency of temperature is improved with the increment of thickness of the TFS. Large capability of heat storage plays an important role in this change. The trend of the temperature variation in the BFS is slightly identical to the temperature in the TFS. The maximum temperature in the BFS increased with the increment of the thickness of TFS, as provided in Table 7.

When only thermal load is applied, the force conditions in the structure, where maximum thermal stress mainly appears in the location of the lattice-frame near the TFS or BFS, are extremely identical to the above

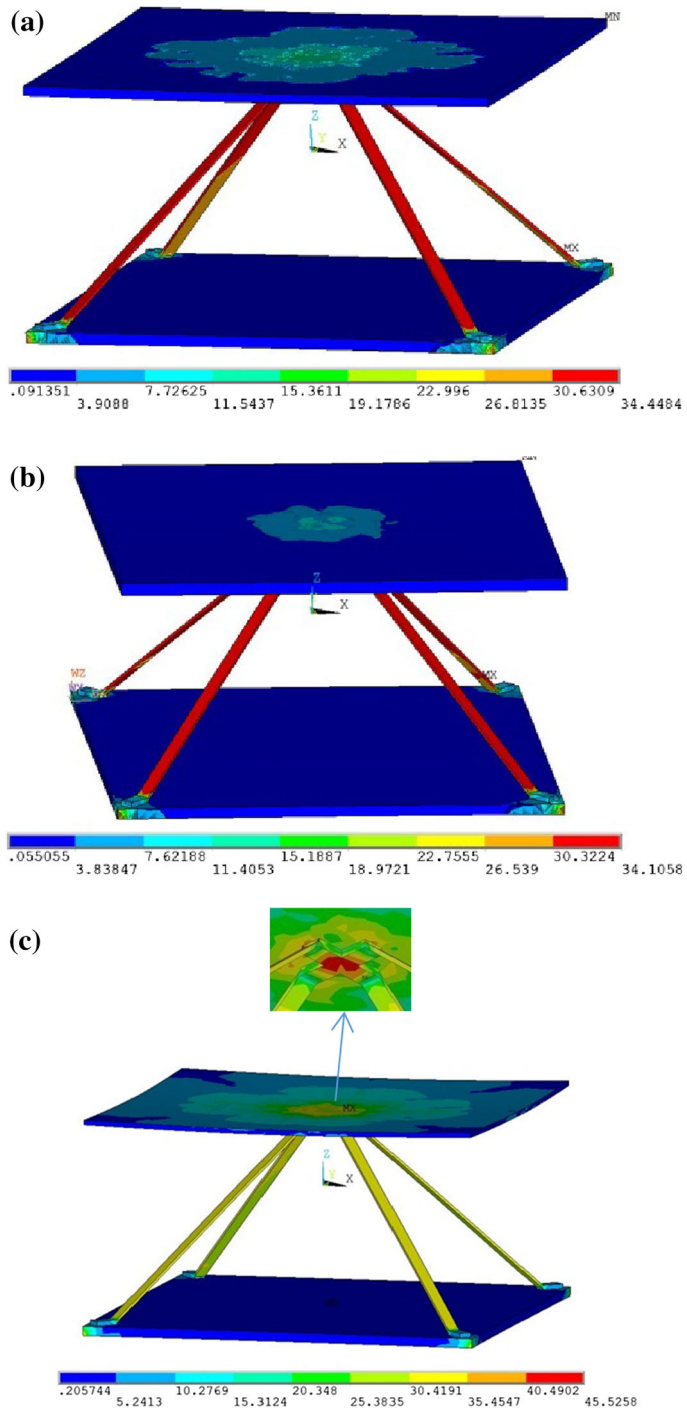

Fig. 14 Von Mises stress contour: **a** in the additional aerodynamic load of 15,000 Pa with 5 mm of $\mathbf{T}_t$ (the maximum stress appears in the whole lattice-frame); **b** in the additional aerodynamic load of 15,000 Pa with the with 7 mm of $\mathbf{T}_t$ (the maximum stress appears in the whole lattice-frame); **c** in the additional aerodynamic load of 15,000 Pa with 3 mm of $\mathbf{T}_t$ (the maximum stress appears in the top part of the lattice-frame near the TFS)

mentioned in last several sections. As shown clearly in Fig. 14, the maximum stress induced by aerodynamic load of 15,000 Pa mainly appears in the lattice-frame. With the increase of thickness for TFS, the location in which the maximum stress appears moves from the upper part of the lattice-frame to the middle position. The stress nearly maintains the same value exceeding the thickness 4 mm for TFS. It can be determined that

Table 8 Maximum temperature in the BFS and stress induced by heat flux and aerodynamic load with the variation of l

Length of the connection (mm)	Temperature/K	Thermal stress/(MPa)	$Stress_{15,000\,Pa}$ /(MPa)	$Stress_{30,000\,Pa}$ /(MPa)	Relative density/(kg/m^3)
10	404.850	3.762	49.440	99.739	220.075
12.5	405.459	3.374	60.055	121.122	220.122
15	405.373	3.429	45.526	92.292	220.165
17.5	405.257	3.551	56.903	115.037	220.204
20	405.201	4.116	50.687	101.813	220.239
22.5	405.117	4.736	53.159	107.222	220.270

Table 9 Relative density for four selected appreciate material combinations

Material combination	Nextel–Nextel–Nextel	Inconel–zirconia–zirconia	Inconel–zirconia–titanium	Inconel–zirconia–beryllium
Relative density (kg/m^3)	245.25	513.23	436.39	320.91

the thickness of 4 mm for TFS can make for a lightweight pyramidal core sandwich panel with an excellent capability of load-bearing and heat insulation. The ITPS can be safely applied in the aircrafts suffering from high aerodynamic heating in the aerodynamic load of 30,000 Pa.

The design variable l represents the length of the connection between the panel and the lattice-frame. The stress under aerodynamic load of 15,000 Pa is fluctuant with the increase of l. It can be observed clearly that variation for l has little effect on the maximum temperature in the BFS and the relative density of the whole structure, as shown in Table 8. Therefore, 15 mm for l is selected for the pyramidal structure to achieve the best thermal–mechanical performance. The maximum stress mainly appears in the upper connection near the TFS as the above-mentioned sections.

The geometric size of the pyramidal core sandwich panel is determined ultimately with additional three material combinations, as provided in Table 9. It can be clearly seen that the whole thermal protection structure with the first material combination can be lightest among these selected material combinations. The last material combination can attain the best heat insulation among all appropriate four material combinations chosen for our research. In the context of aircraft design, many factors should be taken into account, such as weight, mechanical property, as well as price. In the current study, only some basic requirements mentioned are concerned to obtain appropriate material and geometric size. These material combinations above mentioned can be applied in the different parts of hypersonic aircrafts which suffered various thermal conditions and aerodynamic loads.

7 Conclusion

Applied with a typical transient thermal flux, a thermal transfer analysis for the pyramidal core sandwich panel is carried out. The core of the pyramidal core sandwich panel is homogenized and calculated with specific mixtures equations mentioned above. The three-dimensional model can be simplified to two-dimensional model to reduce computational costs for material combination selections. The approximate response surface is fitted and verified adopting considerable samples obtained from 2D heat transfer finite analysis model which has been established. In preliminary design process, some material combinations are selected as candidates for optimization in size according to thermal and mechanical properties which should be satisfied. Several essential design variables on thermal–mechanical properties of the pyramidal structure are investigated to achieve the best performance. Then, the pyramidal core sandwich panel is optimized for several material combinations above mentioned, and a discussion about the optimization results for every appropriate material combination is performed. In general, a lightweight ITPS with excellent capability of load-bearing and heat insulation is achieved after the current research.

Acknowledgments This work was supported by National Natural Science Foundation of China (11202164), by Specialized Research Fund for the Doctoral Program of Higher Education of China (20116102120021).

References

1. Tobe, R.J., Grandhi, R.V.: Hypersonic vehicle thermal protection system model optimization and validation with vibration tests. Aerosp. Sci. Technol. **28**, 208–213 (2013)
2. Spinnler, M., Edgar, R.F., Viskanta, R.: Studies on high-temperature multilayer thermal insulations. Int. J. Heat Mass Transf. **47**, 1305–1312 (2004)
3. Fatemi, J., Lemmen, M.H.J.: Effective thermal and mechanical properties of honeycomb core panels for hot structure applications. AIAA J. Spacecr. Rocket. **46**, 514–525 (2009)
4. Hütter, G., Mühlich, U., Kuna, M.: Micromorphic homogenization of a porous medium: elastic behavior and quasi-brittle damage. Continuum Mech. Thermodyn. **27**, 1059–1072 (2015)
5. Gori, F., Corasaniti, S., Worek, W.M., Minkowycz, W.J.: Theoretical prediction of thermal conductivity for thermal protection system. Appl. Therm. Eng. **49**, 124–130 (2012)
6. Ferraiuolo, M., Manca, O.: Heat transfer in a multi-layered thermal protection system under aerodynamic heating. Int. J. Therm. Sci. **53**, 56–70 (2012)
7. Xie, G., Wang, Q., Zhang, W., Sunden, B., Lorenzini, G.: Optimization design and analysis of multilayer lightweight thermal protection structures under aerodynamic heating conditions. ASME J. Thermal Sci. Eng. Appl.**5**, (2013) Paper no. 011011
8. Ji, T., Zhang, R., Sunden, B., Xie, G.: Investigation on thermal performance of high temperature multilayer insulations for hypersonic vehicles under aerodynamic heating condition. Appl. Therm. Eng. **70**, 957–965 (2014)
9. Li, W., Huang, H., Ai, B., Zhang, Z.: On the novel designs of charring composites for thermal protection application in reentry vehicles. Appl. Therm. Eng. **93**, 849–855 (2015)
10. Kumar, S., Mahulikar, S.P.: Selection of materials and design of multilayer lightweight passive thermal protection system. ASME J. Thermal Sci. Eng. Appl. **8**, 021003 (2016)
11. Huo, L., Cheng, X., Yang, T.: Aerothermoelastic response analysis for C/SiC panel of ceramic matrix composite shingle thermal protection system. Adv. Space Res. **55**, 2352–2371 (2015)
12. Vaz Jr., M., Andrade, F.M.: Pires. A note on the thermal effects upon a Gurson-type material model. Contin. Mech. Thermodyn. **28**, 785–798 (2016)
13. Ranut, P.: On the effective thermal conductivity of aluminum metal foams: review and improvement of the available empirical and analytical models. Appl. Therm. Eng. **87**, 345–374 (2015)
14. Deshpande, V.S., Fleck, N.A., Ashby, M.F.: Effective properties of the octet-truss lattice material. J. Mech. Phys. Solids **49**, 1747–1769 (2001)
15. Prithivirajan, M., Haney, M., Grandhi, R.: Topology optimization of a curved thermal protection system, 47thA-IAA/ASME/ASCE/AHS/ASC Structures, Structural Dynamics, and Materials Conference, AIAA 2006-1982
16. Martinez, O.A., Sankar, B.V., Haftka, R.T., Bapanapalli, S.K., Blosser, M.L.: Micromechanical analysis of composite corrugated-core sandwich panels for integral thermal protection systems. AIAA J. Spacecr. Rocket. **45**, 2323–2336 (2007)
17. Bezazi, A., Remillat, C., Innocenti, P., Scarpa, F.: In-plane mechanical and thermal conductivity properties of a rectangular-hexagonal honeycomb structure. Compos. Struct. **84**, 248–255 (2008)
18. Gogu, C., Bapanapalli, S.K., Haftka, R.T., Sankar, B.V.: Comparison of materials for an integrated thermal protection system for spacecraft reentry. AIAA J. Spacecr. Rocket. **46**, 501–513 (2009)
19. Martinez, O.A., Sharma, A., Sankar, B.V., Haftka, R.T., Blosser, M.L.: Thermal force and moment determination of an integrated thermal protection system. AIAA J. Spacecr. Rocket. **48**, 119–128 (2010)
20. Ravishankar, B., Sharma, A., Sankar, B. V., Haftka, R. T.: Homogenization of sandwich panels with complex microstructure, 18th International Conference on Composite Materials, ICCM 2016, January 18–19, 2016, London, UK
21. Jänicke, R., Diebels, S., Sehlhorst, H.G., Düster, A.: Two-scale modeling of micromorphic continua. Continuum Mech. Thermodyn. **21**, 297–315 (2009)
22. Liu, D., Jin, L., Shang, X.: Comparisons of equivalent and detailed models of metallic honeycomb core structures with in-plane thermal conductivities. Procedia Eng. **31**, 967–972 (2012)
23. Xie, G., Wang, Q., Sunden, B., Zhang, W.: Thermomechanical optimization of lightweight thermal protection system under aerodynamic heating. Appl. Therm. Eng. **59**, 425–434 (2013)
24. Arabnejad, S., Pasini, D.: Mechanical properties of lattice materials via asymptotic homogenization and comparison with alternative homogenization methods. Int. J. Mech. Sci. **77**, 249–262 (2013)
25. Jiang, F., Yu, W., Kerans, R., Chen, M.: Analysis of reusable integrated thermal protection panel elements with various insulating core options, 55th AIAA/ASME/ASME/ASCE/AHS/ASC Structures, Structural Dynamics, and Materials Conference, AIAA 2014-0351
26. Zhao, S., Li, J., Zhang, C., Zhang, W., Lin, X., He, X., Yao, Y.: Thermo-structural optimization of integrated thermal protection panels with one-layer and two-layer corrugated cores based on simulated annealing algorithm. Struct. Multidiscipl. Optim. **51**, 479–494 (2015)
27. Cheng, X., Wei, K., He, R., He, Y., Pei, Y., Fang, D.: The equivalent thermal conductivity of lattice core sandwich structure: a predictive model. Appl. Therm. Eng. **93**, 236–243 (2015)
28. Dorsey, J.T., Poteet, C.C., Wurster, K.E., Chen, R.R.: Metallic thermal protection system requirements, environments, and integrated concepts. AIAA J. Spacecr. Rocket. **41**, 162–173 (2004)
29. Poteet, C.C., Abu-Khajeel, H., Hsu, S.Y.: Preliminary thermal-mechanical sizing of a metallic thermal protection system. AIAA J. Spacecr. Rocket. **41**, 173–183 (2004)
30. Bapanapalli, S.K., Martinez, O.A., Gogu, C., Sankar, B.V., Haftka, R.T., Blosser, M.L.: Analysis and design of corrugated core sandwich panels for thermal protection systems of space vehicles,47th AIAA/ASME/ASCE/AHS/ASC Structures, Structural Dynamics, and Material Conference, 1–4 May 2006, Newport, Rhode island, USA. AIAA 2006-1942
31. Francois, C.: Materials Handbook: A Concise Desktop Reference. Springer, New York (2008)